UDC 520.88

CORRECTION OF SOLAR DOPPLERGRAMS' LARGE-SCALE FLATFIELD

I. Patrickeyev[1], G. Mashnich[2], A. Khlystova[2], H. Zhang[3]

The authors have proposed and compared three different methods of large-scale flatfield correction (time averaging, Fourier filtering, and wavelet-based filtering). As an example, the real dopplergram of the velocity field in a solar active region obtained at the Huairou Solar Observing Station of National Astronomical Observatories of China has been processed. It is shown that any of the applied methods can improve the visual quality of the image. A quantitative comparison of the proposed methods was performed by evaluating the heterogeneity of the images.

1. Introduction. Modern astronomical observations widely use detectors based on a CCD-matrix. There are many papers which discuss not only the features of CCD-detectors, but also the means of overcoming their instrumental distortions. The most essential intensity variations introduced by measuring systems are caused by the following factors: the non-uniform sensitivity of matrix pixels, the non-uniform light field because of the optical irising, the interference or the dust particles on the camera lenses, and the filter defects. Moreover, the intensity varies from frame to frame due to the variations of the diffuse light and the visibility conditions. In the observations of the elongated bright objects such as the Sun, the images obtained outside the focal plane are often used as a flatfield. In this case, the flatfield and the observation data are obtained at the different configurations of an optical system. A calibration method of the spatial non-uniformity of the matrix is proposed in [1]. In this paper, the construction of a flatfield is carried out as follows: the authors first determine the pixel gain coefficients based on the images with known shift and then calculate the flatfield for the whole image by an iteration technique.

Our methods of 2D FeI λ5324.19Å and Hβ Dopplergram processing have been used at the Huairou Solar Observing Station [2, 3]. It was suggested that a flatfield can be described by a surface of the second order. Better results were obtained by subtracting the flatfield of the image calculated by extrapolating and interpolating the flatfield for a limited number of points of the unprocessed image obtained after large-scale averaging. A filtering of the radio maps with the discrete Daubechi wavelets was discussed in [4] and an advantage of the wavelet application over the traditional filtering technique was shown. An estimation of the α-effect based on the velocity field observations and its reliability was discussed in [5].

The main aim of this paper is to show the possibility of the flatfield correction in the obtained time series of the images and to propose other methods of the large-scale flatfield correction based on the truncated Fourier series and the expansion in terms of the continuous wavelet basis.

2. Methods of large-scale flatfield correction. Unfortunately, at present it is impossible to use the flatfield obtained directly in an observation (the so-called "zero frame"), because this will require updating of the software installed on board the observing station. All the methods proposed in this paper do not use a zero frame and are based on different hypotheses of the temporal or the spatial structure of the flatfield. Moreover, all methods use the assumption that the observed image is formed by combining a large-scale flatfield with the ideal velocity field. Therefore, we take into account an additive component only. However, it should be noted that the proposed methods can also be adopted for a multiplicative component correction (by converting the intensity to the logarithmic scale).

2.1. Time Averaging. Let us assume that the flatfield is a stationary structure. The definition "stationary" has a special meaning in the theory of the stochastic processes. In this paper we use this term in a common sense, i.e., "stationary" means time invariable. This assumption looks reasonable at least in the case of an instrumental flatfield. If the velocity field varies with time, then the flatfield and the velocity fields can be separated on the basis of a different behavior of the fields in time. The one way to identify stationary structures is to collect frames of the same active region and then to perform averaging. Such a mean frame involves structures reproduced

[1] Institute of Continuum Mechanics, Russian Academy of Sciences, Korolyova 1, 614013, Perm, Russia; e-mail: pat@icmm.ru

[2] Institute of Solar and Terrestrial Physics, Russian Academy of Sciences, Lermontova 126, 664033, Irkutsk, Russia; e-mail: mashnich@iszf.irk.ru, ancha-k@nm.ru

[3] National Astronomical Observatories, Chinese Academy of Sciences, 100012, Beijing, China; e-mail: hzhang@bao.ac.cn

in each frame as well as the time averaged non-stationary structures. Therefore, if the velocity at a point is governed by a random time function with zero mean value, then the point in the mean frame will have the zero velocity value.

The mean frame can be found by the following formula: $f_{i,j} = \dfrac{1}{N}\sum\limits_{n=0}^{N-1} s_{i,j}^{(n)}$, where N is the number of the frames, i, j are the indices of a pixel in the x- and y-axes, respectively, $s_{i,j}$ are the frames, and (n) is a frame number.

The corrected velocity field is obtained by subtraction of the mean frame from the observed velocity frame. A degree of separation of the velocity field and flatfield increases with the number of frames; however, the observation time cannot be too long. In practice, acceptable results are achieved even at $N = 15-20$.

2.2. Fourier Filtering. The application of the Fourier transform to the flatfield filtering [6] relies on the assumption that the flatfield and the velocity field have different spectral features. Since the flatfield has a low-frequency spectrum and the velocity field spectrum involves mainly the middle and high frequencies, it is possible to separate them in the frequency domain. The visual analysis of the frames shows that the typical flatfield appears as a structure consisting of a few large spots or of the two or three wide strips extending across the whole frame area. To delete the low-frequent structure, it is necessary to apply the 2D Fourier transform and to replace the Fourier coefficients at the lowest frequencies by zeros. The acceptable results are achieved after deleting the 2 or 3 lowest frequencies.

The 2D Fourier coefficients are obtained from the formula

$$\widehat{s}_{k_x,k_y} = \frac{1}{N_x N_y}\sum_{i=0}^{N_x-1}\sum_{j=0}^{N_y-1} s_{i,j} e^{-2\pi\sqrt{-1}(k_x i/N_x + k_y racj/N_y)},$$

where N_x and N_y are the x- and y-image dimensions in the physical space; k_x and k_y are the coordinates in the frequency domain.

2.3. Wavelet Filtering. A continuous wavelet transform [7] allows us to obtain almost the same result as the Fourier transform. Following the initial assumption, the flatfield can be considered as a large-scale structure, whereas the velocity field — as a combination of the middle-scale and the small-scale structures. The 2D isotropic wavelet transform coefficients are obtained according to the formula

$$\widetilde{s}_{a,i',j'} = a^{-1}\sum_{i=0}^{N_x-1}\sum_{j=0}^{N_y-1} s_{i,j}\psi^*\Big(\frac{i-i'}{a}, \frac{j-j'}{a}\Big),$$

where a, i', and j' are the parameters of the scaling and the translation along the x- and y-axes, respectively, ψ is a wavelet, and $*$ indicates complex conjugation.

A flatfield image is obtained by the synthesis (inverse wavelet transform) on the largest scales. The subtraction of the flatfield from the original image yields the filtered image. In this paper, the Mexican Hat wavelet is used:

$$\psi(x,y) = (2 - x^2 - y^2)\exp\big(-(x^2+y^2)/2\big).$$

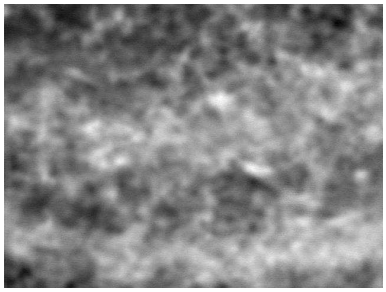

Fig. 1. The original velocity field

Here the wavelet coefficients are calculated as a linear convolution of the original image by the wavelet series whose scale varies from 1 pixel to the image size. The synthesis is made using the Morlet formula [8]. In contrast to the Fourier-based method with a sharp frequency cut-off, the wavelet-based method gives smooth borders of the frequency bandwidth [9].

3. Numerical results. All the methods described above were applied to the real Dopplergrams obtained at the Huairou Solar Observing Station.

Each Dopplergram is obtained by the formula

$$V_{\text{dop}} \sim \frac{\sum\limits_{n=1}^{256} I_{\text{red}} - \sum\limits_{n=1}^{256} I_{\text{blue}}}{\sum\limits_{n=1}^{256} I_{\text{red}} + \sum\limits_{n=1}^{256} I_{\text{blue}}},$$

where I_{red} and I_{blue} are the measured intensities in the red and blue wings of the spectral line. Each pair is separated in time by 20 ms.The time period of collection is about 40 s.

Figure 1 illustrates a typical velocity field obtained at the $H\beta$ wavelength λ equal to 486.1 nm. Some results of the large-scale correction are presented in Figures 2a, 3a, and 4a. The flatfields obtained by different methods are given in Figures 2b, 3b, and 4b. Each filtered image is calculated as a result of the subtraction of the corresponding flatfield from the velocity field 1, whereas each filtered image looks more or less homogeneous, without large-scale structures.

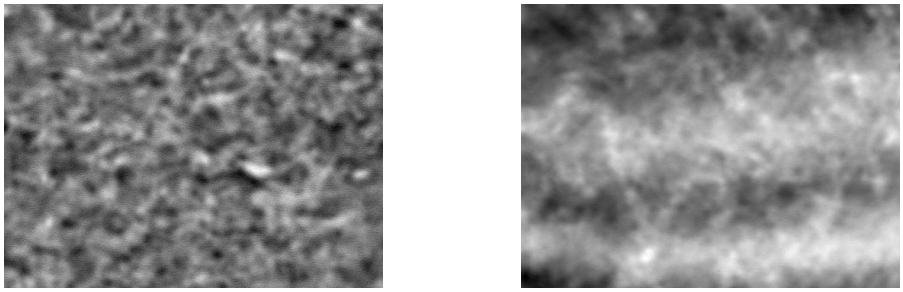

Fig. 2. Time averaging: a) filtered image; b) flatfield

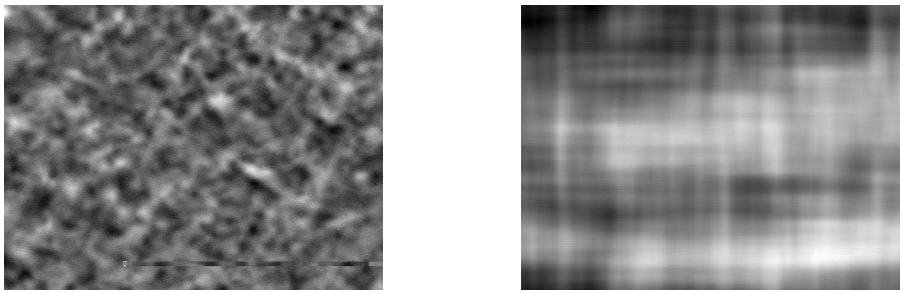

Fig. 3. Filtering in the frequency domain: a) filtered image; b) flatfield obtained with FFT

The results obtained by the mean frame method are presented in Figure 2. A filtered image (Figure 2a) was obtained by subtracting the mean frame from the original image. The corresponding flatfield (Figure 2) is the result of the averaging of 23 frames over a period of 9 minutes. Our comparison with the original image shows that the flatfield distortions become almost invisible.

Figure 3 illustrates the results of the image processing with the Fourier transform. The large-scale structures were filtered almost completely out; however, the flatfield image obtained with the FFT (Figure 3b) differs from the mean frame (Figure 2b).

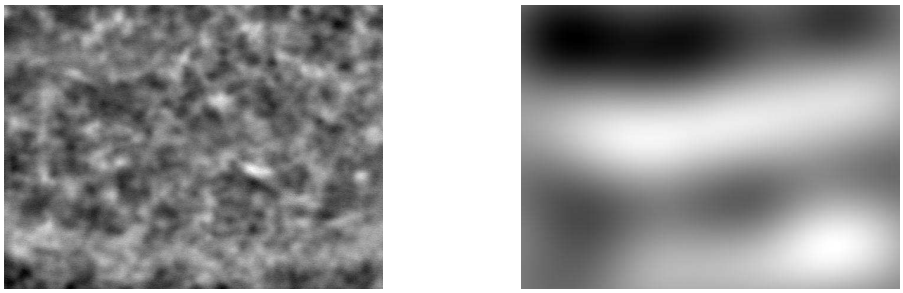

Fig. 4. Wavelet filtering: a) filtered image; b) flatfield obtained with wavelets

Some results of the wavelet-based filtering is presented in Figure 4. Similarly to the previous cases, the filtering yields a visible improvement of the image quality, which can be seen as a more uniform distribution of the intensity over the frame field. The flatfield image obtained by a synthesis of the large-scale wavelets (Figure 4b) seems to be the smoothest one compared to the other flatfield images.

A simple quantitative estimation of the image homogeneity can be done by comparing the mean values in the upper and lower halves of the image. It is expected that the perfectly homogeneous image has the same mean value in both parts. In order to make a quantitative comparison of the above methods, the calculated mean values of each half-image were normalized to the mean value of the whole image. The table shows the deviation of the calculated values from the mean value of the whole image for the velocity field (Figure 1) and

for each of the filtered images. The upper (lower) half-image of the original velocity field has the mean values of about 5 % smaller (larger) than the mean value of the whole image. The halves of the filtered images have the mean values weakly deviating in the range from 2.3 % to 0.03 %. Thus, each of the proposed methods can reduce the image heterogeneity by subtracting the corresponding flatfield.

Deviations (in %) of the mean value calculated in halves of the image from the mean value of the whole image

Image		Upper half-image	Lower half-image
Velocity field	(Fig. 1)	-5.5	5.1
Time averaging	(Fig. 2)	-0.1	-0.4
Fourier filtering	(Fig. 3)	-0.03	-0.6
Wavelet filtering	(Fig. 4)	-2.3	1.8

Actually, it is possible to apply more sophisticated methods of the estimation of the image homogeneity (the calculation of the correlation radius, etc.). Perhaps, we do not need to use such methods if one can say that the images have no large-scale structures. Indeed, the aim of the proposed methods is making an image free of the instrumental artifacts (not making them completely homogeneous). As a result, now we have three similar images; each image looks adequately enough for the further analysis of the velocity distribution.

4. Conclusion. From the visual estimation of the filtered images it may be concluded that the acceptable results can be obtained using any of the proposed methods. The time averaging method yields acceptable results in studying the structure evolution over the time intervals comparable with the observation time of a single image series. The advantage of the Fourier-based and th wavelet-based methods is the possibility of processing a single image, whereas the mean frame method requires a series of the images. If a zero frame is known, an optimized filter should be used; this gives a further improvement of the Fourier-based method. The wavelet-based filtering can also be improved by choosing the other wavelets for the analysis and the synthesis. For example, the directional structures can be better filtered with the anisotropic wavelets [10].

Acknowledgements. The authors would like to thank V. V. Grechnev, D. D. Sokoloff, P. G. Frick, K. M. Kuzanyan for the fruitful discussions. This work was partially supported by the collaborative grants of RFBR and NSFC 02–02–39027, RFBR and DFG 03–02–04031, the grant RFBR 03–02–16384, the State Support of Leading Scientific Schools of the Russia Federation, the grant SS–733.2003.2, and the Exchange Program for Scientists' visits between the Russian Academy of Sciences and the Chinese Academy of Sciences. The Russian authors would like to thank the Huairou Solar Observing Station of the National Astronomical Observatories of China for hospitality.

References

1. *Kuhn J., Lin H., Loranz D.* Gain calibrating nonuniform image-array data using only the image data // Publications of the Astronomical Society of the Pacific. 1991. **103**. 1097–1108.
2. *Ai G., Li W., Zhang H.* Formation of the FeI 5324.19 line in the Sun and theoretical calibration of solar magnetic telescope // Chinese Journal of Astronomy and Astrophysics. 1992. **6**. 129–136.
3. *Zhang H., Ai G.* The formation of the H-Beta line in the solar chromosphere magnetic field // Acta Astronomica Sinica. 1986. **27**. 286.
4. *Chen P., Zhang X., Xiang S., Feng L., Reich W.* Protruding structure buried in radio map by wavelet // Chinese Physics Letters. 2000. **17**, N 5. 388–389.
5. *Zhang H., Bao S., Kuzanyan K.* Twist of magnetic fields in solar active regions // Astronomy Reports. 2002. **46**, N 5. 424–434.
6. *Bracewell R.* Fourier transform and its application. New York: McGrow-Hill, 1965.
7. *Farge M., Hunt J.C.R., Vassilicos J.C.* Wavelets, fractals and Fourier transforms. Oxford: Clarendon Press, 1993.
8. *Daubechies I.* Ten lectures on wavelets. Philadelphia: SIAM, 1992.
9. *Frick P., Beck R., Berkhuijsen E., Patrickeyev I.* Scaling and correlation analysis of galactic images // Monthly Notices of the Royal Astronomical Society. 2001. **327**. 1145–1157.
10. *Patrickeyev I., Fletcher A., Beck R., Berkhuijsen E., Frick P., Horrelou C.* Anisotropic wavelet analysis of spiral arms and magnetic fields in the galaxy M51 // The Magnetized Plasma in Galaxy Evolution (Proceedings of the Conference held in Cracow, Poland, Sept. 27th - Oct. 1st, 2004. Edited by K. Chyzy, K. Otmianowska-Mazur, M. Soida, and R.-J. Dettmar). Cracow, 2005. 130–135.

Received 09 September 2005